Dynamics of concurrent and sequential Central European and Scandinavian heatwaves

Author(s):
Spensberger, Clemens; Madonna, Erica; Boettcher, Maxi; Grams, Christian M.; Papritz, Lukas; Quinting, Julian F.; Röthlisberger, Matthias; Sprenger, Michael; Zschenderlein, Philipp

Publication date:
2020-10

Permanent link:
https://doi.org/10.3929/ethz-b-000422251

Originally published in:
Quarterly Journal of the Royal Meteorological Society 146(732), https://doi.org/10.1002/qj.3822

Funding acknowledgement:
787652 - An integrated weather-system perspective on the characteristics, dynamics and impacts of extreme seasons (EC)

Received: 9 December 2019 | Revised: 15 April 2020 | Accepted: 27 April 2020 | Published on: 15 June 2020

DOI: 10.1002/qj.3822

Quarterly Journal of the Royal Meteorological Society RMetS

RESEARCH ARTICLE

Dynamics of concurrent and sequential Central European and Scandinavian heatwaves

C. Spensberger[1] | E. Madonna[1] | M. Boettcher[2] | C. M. Grams[3] | L. Papritz[2] | J. F. Quinting[3] | M. Röthlisberger[2] | M. Sprenger[2] | P. Zschenderlein[3]

[1]Geophysical Institute, University of Bergen and Bjerknes Centre for Climate Research, Bergen, Norway

[2]Institute for Atmospheric and Climate Science, ETH Zurich, Zurich, Switzerland

[3]Institute of Meteorology and Climate Research (IMK-TRO), Department of Troposphere Research, Karlsruhe Institute of Technology, Karlsruhe, Germany

Correspondence
C. Spensberger, Geophysical Institute, University of Bergen, Postboks 7803, 5020 Bergen, Norway.
Email: clemens.spensberger@uib.no

Funding information
Deutsche Forschungsgemeinschaft, Grant/Award Number: SFB/TRR 165; H2020 European Research Council, Grant/Award Number: 787652; Helmholtz Association, Grant/Award Number: VH-NG-1243

Abstract

In both 2003 and 2018 a heatwave in Scandinavia in July was followed by a heatwave in Central Europe in August. Whereas the transition occurred abruptly in 2003, it was gradual in 2018 with a 12-day period of concurrent heatwaves in both regions. This study contrasts these two events in the context of a heatwave climatology to elucidate the dynamics of both concurrent and sequential heatwaves. Central European and, in particular, concurrent heatwaves are climatologically associated with weak pressure gradient (WPG) events over Central Europe, which indicate the absence of synoptic activity over this region. One synoptic pattern associated with such events is Scandinavian blocking. This pattern is at the same time conducive to heatwaves in Scandinavia, thereby providing a mechanism by which Scandinavian and Central European heatwaves can co-occur. Further, the association of WPG events with Scandinavian blocking constitutes a mechanism that allows heatwaves to grow beyond the perimeter of the synoptic system from which they emanated. A trajectory analysis of the source regions of the low-level air incorporated in the heatwaves indicates rapidly changing air mass sources throughout the heatwaves in both regions, but no recycling of heat from one heatwave to the other. This finding is line with a composite analysis indicating that transitions between Scandinavian and Central European heatwaves are merely a random coincidence of heatwave onset and decay.

KEYWORDS

block, Central Europe, heatwave, Scandinavia, weak pressure gradient

1 | INTRODUCTION

The 2018 summer was amongst the hottest in the recorded history of Europe (Magnusson *et al.*, 2018), with large parts of Scandinavia (Sinclair *et al.*, 2019) and Central Europe affected by a heatwave (e.g., Vogel *et al.*, 2019). Long periods of high temperatures with reduced precipitation are not only a threat for human life (e.g., Robine *et al.*, 2008), but can also cause crop failure and increase the hazard of forest fires (e.g., De Bono *et al.*, 2004; Lesk *et al.*, 2016). The year 2018 was anomalously warm and dry in both spring and summer (Kennedy *et al.*, 2019). In terms of

amplitude, persistence, and spatial extent, the 2018 heatwaves were comparable to the two prominent heatwaves in 2003 and 2010 over Europe and Russia, respectively (Barriopedro *et al.*, 2011; Fischer, 2014). In those summers, more than one million square kilometres were simultaneously affected by a heatwave (Barriopedro *et al.*, 2011).

Despite the prominence of heatwaves in current research, there is still no commonly agreed-upon definition in the literature. Most definitions include temperature exceeding at least one particular threshold and a persistence criterion, that is, the threshold must be exceeded for several consecutive days (the review paper of Perkins, 2015 gives more information). Most studies consider daily temperatures (e.g., Meehl and Tebaldi, 2004; Fischer and Schär, 2010; Russo *et al.*, 2014), but sometimes monthly values are used (e.g., Coumou and Robinson, 2013). Moreover, some studies consider the average over a season of all grid points that fulfill the chosen criteria, but do not require the affected areas to be connected in space and time (e.g., Coumou and Robinson, 2013; Vogel *et al.*, 2019). In such a case, several spatially and temporally unrelated heat extremes can account for the seasonal signal. The aspect that we aim to address in this study is the dynamical link between the transition from one heatwave to another. Hence, for this study we are interested in heatwaves that are spatially and temporally related, meaning that they have to occur in the vicinity of each other, and be separated by at most a few days.

Summer heat extremes are often associated with atmospheric blocks, stationary and persistent anticyclones (e.g., Black *et al.*, 2004; Trigo *et al.*, 2005; Dole *et al.*, 2011; Pfahl and Wernli, 2012; Stefanon *et al.*, 2012; Jézéquel *et al.*, 2018b). Consequently, heat extremes often arise in blocked weather regimes (e.g., Cassou *et al.*, 2005; Schaller *et al.*, 2018). Warm surface conditions arise from the combined effect of subsidence, diabatic heating, and, to a smaller extent, warm-air advection (Black *et al.*, 2004; Trigo *et al.*, 2004; Bieli *et al.*, 2015; Horton *et al.*, 2016; Quinting and Reeder, 2017; Zschenderlein *et al.*, 2019). Further, the lack of precipitation and soil moisture deficits can precondition extreme surface temperatures (Fischer *et al.*, 2007; Vautard *et al.*, 2007; García-Herrera *et al.*, 2010; Miralles *et al.*, 2014). Due to the persistence and stationarity of a block, the temperature anomalies can build up over time and lead to heatwaves of different intensity. However, they remain limited in size by the spatial extent of the anticyclone.

There is no evidence that the dynamical link between summer heatwaves and atmospheric blocking will change with global warming (Schaller *et al.*, 2018). However, several studies observe and foresee an increase in the frequency and spatial extent of heatwaves (e.g., Meehl and Tebaldi, 2004; Fischer and Schär, 2010; Russo *et al.*, 2014; Christidis *et al.*, 2015; Russo *et al.*, 2015; Vogel *et al.*, 2019), whereas there is little evidence for significant changes in the frequency of summer blocking, neither during the last decades (Barnes *et al.*, 2014) nor in future climate projections (Schaller *et al.*, 2018; Woollings *et al.*, 2018; Jézéquel *et al.*, 2018a). The size of ridges and thus anticyclones is set by semi-geostrophic dynamics (Hoskins, 1975; Wolf and Wirth, 2015). This size might increase to some extent with climate change with weakening westerlies in the mean state (Nabizadeh *et al.*, 2019), but is likely not enough to explain the discrepancy in the projected change of heatwaves and blocks. The discrepancy might thus result from blocking being more often associated with heatwaves, for example, due to thermodynamic changes, or increasing importance of other mechanisms leading to heatwaves.

The dynamics leading to heatwaves depend on the considered region and have been shown to be more complicated than a one-to-one association with blocking (Sánchez-Benítez *et al.*, 2018; Zschenderlein *et al.*, 2019). For example, Stefanon *et al.* (2012) and Sousa *et al.* (2018) showed that in southern Europe narrow subtropical ridges rather than blocking lead to extremely warm conditions. Rossby-wave packets (Fragkoulidis *et al.*, 2018), recurrent (Röthlisberger *et al.*, 2019) or stationary (Kornhuber *et al.*, 2019) Rossby waves have also been linked to high temperature extremes. Further, Drouard and Woollings (2018) revealed a regional dependence of the formation and maintenance mechanisms of blocking and their connection to the North Atlantic storm track. This could hint at regional variations of the link between heatwaves and blocks (as shown for other regions in Pfahl and Wernli, 2012).

While these studies considered the link between different synoptic features and individual heatwaves, the dynamical mechanisms involved in the concurrent and sequential occurrence of heatwaves in adjacent regions have not yet been considered. As a first step in this direction, we here consider heatwaves in Scandinavia and Central Europe. We aim to highlight the key dynamical features associated with concurrent and sequential heatwaves in these regions. In particular, we address the following questions:

1. Do concurrent heatwaves arise due to the same synoptic system, for example, a single block?
2. In sequential heatwaves, is the transition between regions associated with typical upper- or low-level flow patterns?
3. In heatwave transitions, is low-level heat recycled from one heatwave to the next?

In order to address these questions, we will consider Eulerian and Lagrangian flow features (Sprenger *et al.*, 2017), following the pathway of air parcels (e.g., Quinting *et al.*, 2018). We first contrast the 2018 heatwaves

with the extensively studied cases of 2003 (e.g., Black *et al.*, 2004; Fink *et al.*, 2004; Luterbacher *et al.*, 2004; Schär and Jendritzky, 2004; Cassou *et al.*, 2005; Fischer *et al.*, 2007; García-Herrera *et al.*, 2010). In both 2018 and 2003 a heatwave in Scandinavia in July was followed by a heatwave in Central Europe in August. However, as we will show, in 2003 the onset of the Central European heatwave coincided with the end of the Scandinavian heatwave (sequential occurrence), whereas in 2018 we observed concurrent heatwaves in Scandinavia and Central Europe during a transition phase of nearly two weeks.

The paper is structured as follows. We first introduce some definitions, metrics and data (Section 2) used to document and discuss the dynamics behind the 2018 concurrent heatwaves (Section 3) and contrast them to the sequential heatwaves of 2003 (Section 4). We then generalise some of our findings using a Scandinavian and Central European heatwave climatology (Section 5), and summarize the main findings (Section 6).

2 | METHODS AND DATA

We base our analysis on 6-hourly ERA-Interim reanalyses for the period 1979–2018 (Dee *et al.*, 2011). Unless otherwise noted, we use data from the surface and 60 model levels, interpolated on a horizontal grid with 1° grid spacing. In this dataset, we detect blocks using the Croci-Maspoli *et al.* (2007) scheme. This scheme defines blocks as persistent potential vorticity (PV) anomalies of at least −1.0 PVU in the upper troposphere. The threshold is a compromise between the original threshold of −1.3 PVU suggested by Croci-Maspoli *et al.* (2007), and the "weak block" definition of Pfahl and Wernli (2012) with a threshold of −0.7 PVU.

2.1 | Definition of concurrent and sequential heatwaves

We base our definition of heatwaves on the percentile-based daily heatwave magnitude index (HWMId) of Russo *et al.* (2015). This index applies only to individual grid points, whereas we are interested in detecting heatwaves covering predefined regions. We therefore follow Zschenderlein *et al.* (2019) and extend the original definition of the HWMId. Specifically, we define a heatwave as a period of at least five consecutive days where more than 20% of the land surface in predefined regions exceeds the local 90th percentile of maximum temperatures. The maximum temperatures are based on 6-hourly 2 m temperatures, and the 90th percentile for every grid point is based on a centred 31-day moving window. We apply this definition to a Central European region (CE; 45–55°N, 0–20°E; 1.5 million km^2 land surface) and a Scandinavian region (SC; 55–70°N, 0–30°E; 1.4 million km^2 land surface; regions are shown in Figure 2 below), and to the extended summer season of May to September. The identified heatwave periods are not sensitive to the exact choice of the boxes.

Our heatwave definition complies with the recommendations of Cattiaux and Ribes (2018) in that we select the spatiotemporal scale in an automatic way. Nevertheless, the choice of temporal and spatial thresholds remains subjective. With the given thresholds, we identify 74 heatwaves in Central Europe and 87 heatwaves in Scandinavia during the 40 extended summer periods used in this study.

Further, we define concurrent heatwaves as periods of minimum five consecutive days during which heatwaves are active both in Central Europe and in Scandinavia. Finally, we identify a sequential heatwave event by a CE heatwave onset within ± 3 days of the end of a SC heatwave, or *viceversa*.

2.2 | Trajectory calculation and clustering

In order to determine the origin of near-surface air masses during the 2003 and 2018 heatwaves, we calculate 10-day backward trajectories with the Lagrangian Analysis Tool (LAGRANTO; Wernli and Davies, 1997; Sprenger and Wernli, 2015). As we are interested in the origin of the near-surface air masses, trajectories are initialized at ERA-Interim grid points 10, 30, 50, and 100 hPa above the surface at all 6-hourly time steps and grid points affected by a heatwave. As we require heatwaves to occur over land, we start trajectories only from land grid points.

For extracting characteristic pathways of the near-surface air masses from these trajectories, we use the hierarchical clustering approach of Hart *et al.* (2015), which is outlined briefly as follows. The backward trajectories are stored in a matrix $\mathbf{W}$ which contains J trajectories with N characteristics each. We base the clustering on the horizontal position of the trajectories over time t, that is, their longitude $\lambda(t)$ and their latitude $\phi(t)$. Consequently, $\mathbf{W}$ for trajectory j is defined as

$$\mathbf{W}_j = \left[\lambda_{j,t=0}, \ldots, \lambda_{j,t=T}, \boldsymbol{\phi}_{j,t=0}, \ldots, \boldsymbol{\phi}_{j,t=T}\right]. \quad (1)$$

With $T = 41$ time steps in 10 days using 6-hourly resolution, the vector $\mathbf{W}_j$ has $N = 82$ entries. The hierarchical clustering algorithm then agglomerates in an iterative approach the most similar trajectories into clusters.

Here, the measure of similarity is the Euclidean distance defined as

$$d_{jk} = \sqrt{\sum_{n=1}^{N} \left\{ \mathbf{W}_j(n) - \mathbf{W}_k(n) \right\}^2}, \tag{2}$$

where j and k denote the two trajectories being compared. The iterative process continues until all trajectories are grouped into a single cluster. The optimal number of clusters is assessed following the approach of Hart *et al.* (2015). In this study, it was found to be three for both SC and CE heatwaves.

2.3 | Weak pressure gradient events

During the analyses we noted the prevalence of weather situations characterised by weak pressure gradients (WPGs), in particular for CE and concurrent heatwaves (Section 5.1). Note that this definition is unrelated to the weak pressure gradient approximation in tropical atmospheric dynamics, which is also commonly abbreviated WPG. To define midlatitude WPG events, we consider the magnitude of the local 850 hPa geopotential height gradient $|\nabla_{850} Z|$. A WPG event is then identified at each grid point where

$$|\nabla_{850} Z| < \frac{5 \text{ m}}{100 \text{ km}} = 5 \times 10^{-5}. \tag{3}$$

The dimensionless threshold of 5×10^{-5} was chosen subjectively, but corresponds roughly to the 30th percentile of all $|\nabla_{850} Z|$ values north of 40°N (not shown). In the mid and high latitudes, vanishing gradients in the 850 hPa geopotential height field occur near the centres of anticyclones and sometimes cyclones, as well as in regions of low synoptic activity. However, by considering both WPG features (i.e., the $|\nabla_{850} Z|$ field) as well as the sea-level pressure field, one can easily distinguish between WPG conditions near the centre of synoptic systems and WPG conditions arising due to weak synoptic activity.

The climatological frequency of occurrence of WPG events in and around Europe in summer is depicted in Figure 1. At subtropical latitudes, the climatological summer WPG frequency exceeds 75%, which suggests that this metric identifies subtropical anticyclones as WPG features. Between 40° and 50°N, the climatological WPG frequency decreases from roughly 50–60% to less than 30%. Lowest values (below 10%) are found over the North Atlantic, to the west of the British Isles. All WPG anomalies discussed hereafter are calculated with respect to the climatology shown in Figure 1.

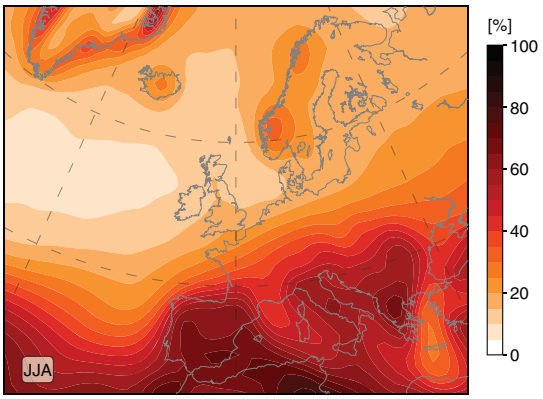

FIGURE 1 Climatological frequency of weak pressure gradient events during the summers (JJA) of 1979–2018

3 | THE 2018 CONCURRENT HEATWAVES

We first turn our attention to the 2018 heatwaves (Figure 2). Kornhuber *et al.* (2019), Drouard *et al.* (2019) and Vogel *et al.* (2019) show that several regions in the Northern Hemisphere were affected by either heat or extreme precipitation. New temperature records were set in many places in Scandinavia and Central Europe (Kornhuber *et al.*, 2019), and in particular Sweden suffered from unprecedented and widespread wildfires (The Local, 2018). Here we focus on the SC heatwave which persisted throughout most of July (10 July–4 August), the subsequent CE heatwave (24 July–9 August), and in particular on the long transition period of concurrent heatwaves in CE and SC (24 July–4 August; heatwave periods and relation to weather regimes are shown in Supporting Information Figure S1b).

The SC heatwave was associated with a persistent trough–ridge couplet centred in the eastern Atlantic (Figure 2a–d), with most of Scandinavia under the influence of the persistent ridge. During most of the heatwave, the PV anomaly associated with that ridge exceeded −1.0 PVU, such that the ridge fulfilled our criteria for a block (Figure 2b,d). Upper-tropospheric flow was generally diverted around the block with pronounced wind speed maxima over the northern Mediterranean and the upstream flank of the ridge in the North Atlantic (Figure 2b,d).

In the beginning of August 2018, the Scandinavian block was displaced northwards and eventually decayed. Accompanying this evolution, the North Atlantic trough weakened, leading to more zonal flow over Great Britain and the North Sea (Figure 2e,f). This ended the 2018 SC heatwave, but allowed a heatwave to emerge over Iberia (Barriopedro *et al.*, 2020). Even after the end of the SC heatwave, Central Europe remained under the influence

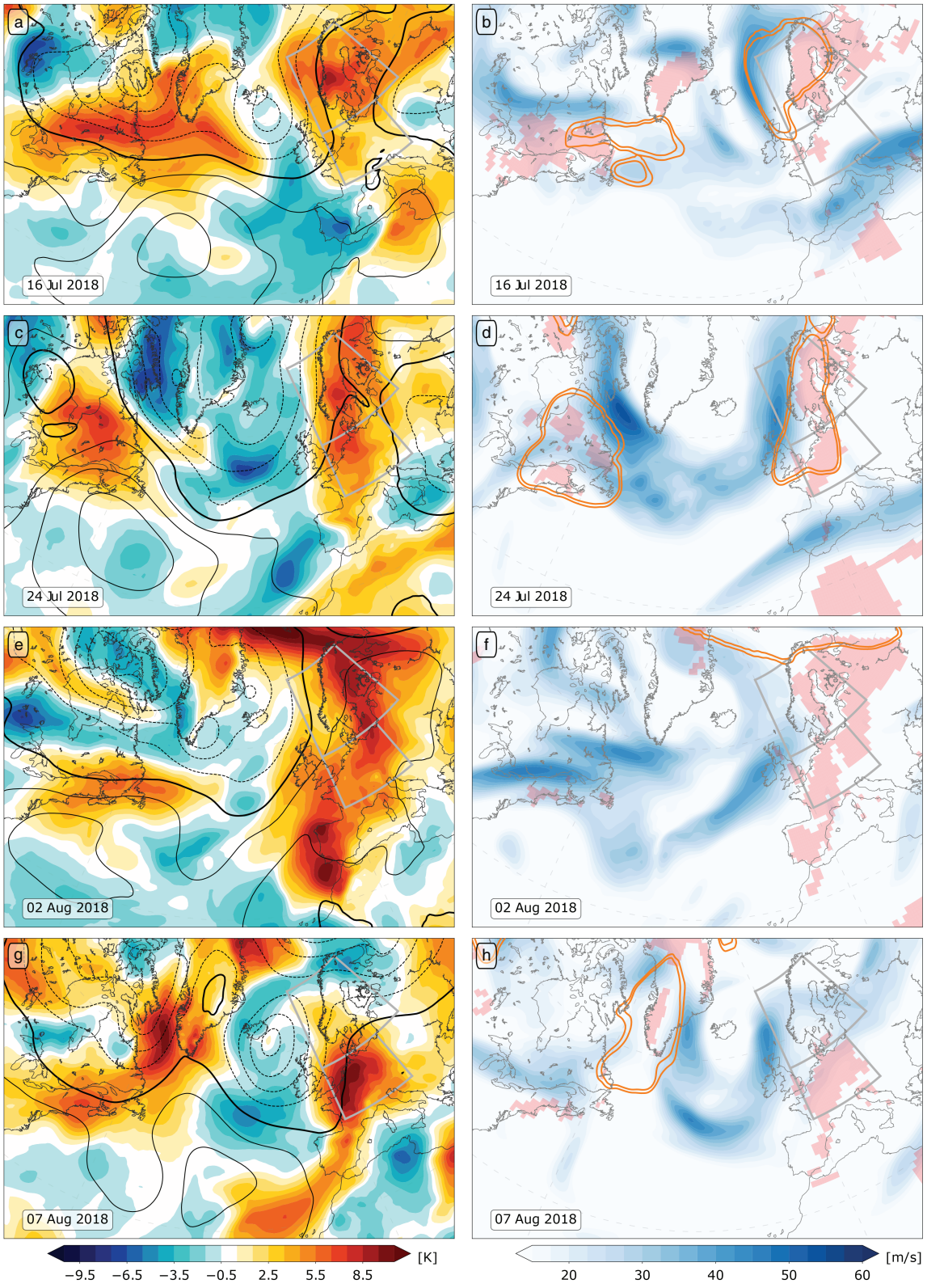

FIGURE 2 Daily mean fields illustrating the synoptic evolution during the 2018 heatwaves. (a, c, e, g) 850 hPa temperature anomalies (K, colour shading) with respect to the 1979–2018 monthly median, and 850 hPa geopotential height (contours with interval 50 m; 1500 m bold, dashed below 1,500 m). (b, d, f, h) Wind speed at 300 hPa ($m \cdot s^{-1}$, shading), occurrence of individual hot days on which we base our heatwave index (pink mask), and PV anomaly-type blocks (orange contours at 0.2 and 0.4 occurrence frequency). (a, b) show a first peak of the SC heatwave (16 July 2018), (c, d) the onset of the concurrent heatwaves (24 July), (e, f) the final peak of the concurrent heatwaves (2 August), and (g, h) a final peak of the CE heatwave (7 August). The grey boxes in all panels indicate the Scandinavian (SC) and Central European (CE) regions used throughout this study

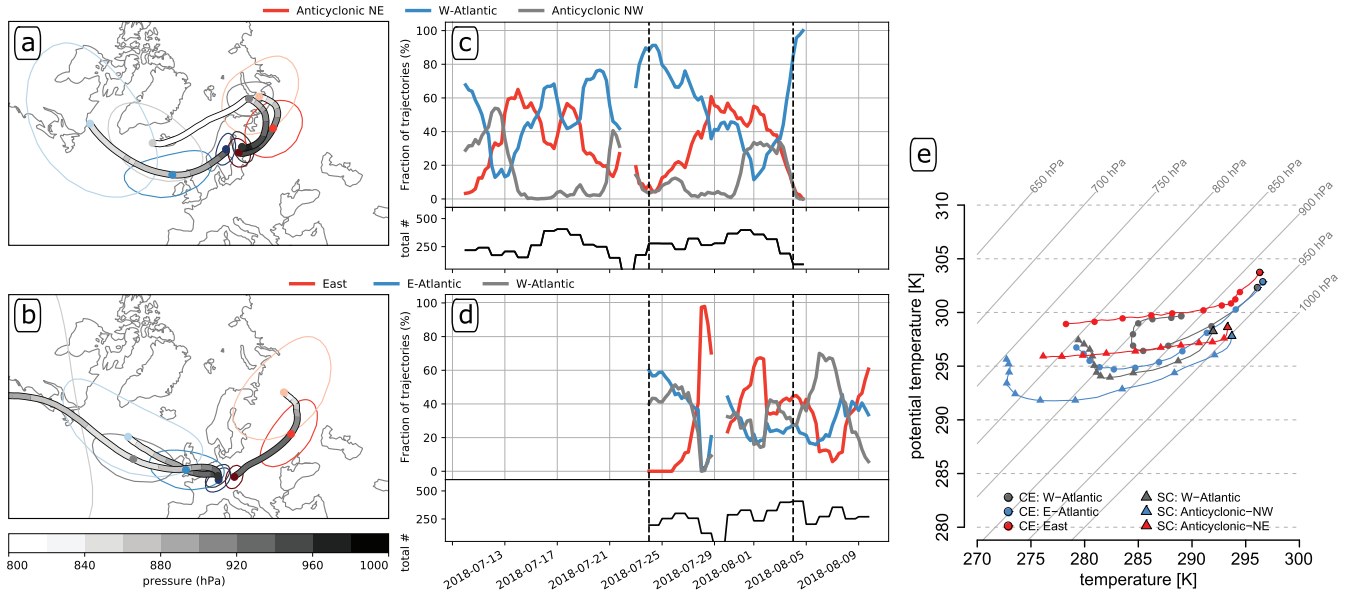

FIGURE 3 (a, b) show cluster median backward trajectories initialised in the 2018 heatwaves coloured by their median pressure (hPa) for (a) SC and (b) CE. Trajectories are initialised at time steps and grid points affected by these heatwaves at 10, 30, 50 and 100 hPa above the surface. The ellipses show the dispersion of the trajectories around their median location (coloured dots) at 10, 5, and 0 days prior to being part of a heatwave, with about 2/3 of the trajectories located inside the ellipses. (c, d) show composition of near-surface air masses for (c) Scandinavia and (d) Central Europe, determined by the cluster analysis in (a, b) and based on 10-day backward trajectories from within the heatwave regions. The black line shows the number of trajectories contributing to the respective analysis, and indicates the spatial extent of the respective heatwave as trajectories are initialised at every affected grid point. (e) shows thermodynamic evolution of cluster trajectories in (a, b). Symbols show daily medians of potential temperature and temperature for the trajectory clusters for the CE (circles) and SC (triangles) regions. Black edges to the symbols indicate the time of arrival in the target area. Isobars (interval 50 hPa) and isentropes (interval 5 K) are shown by grey solid and dashed lines, respectively

of a small-amplitude ridge which diverted the jet and synoptic activity towards Scandinavia (Figure 2g,h). From a weather regime perspective, this is consistent with the observed long-lasting European blocking life cycle which transitioned into a Scandinavian blocking by the end of July (cf. Figure S1b).

During the SC heatwave, the largest temperature anomalies propagated in waves along the Scandinavian coastline, and eventually eastwards and into the high Arctic (Figure 2a,c,e). This signal suggests a contribution of low-level advection from the southwest in the onset and maintenance of the 2018 SC heatwave. Though the air parcels did not necessarily get warmer on their way towards Scandinavia, the poleward movement of the warm air mass led to larger temperature anomalies along its pathway.

A trajectory analysis further illustrates this process (Figure 3a,c). During the onset, as well as in three distinct waves during the heatwave, advection from the southwest was the dominant source of air masses for the SC heatwave (Figure 3c). The composition of the air masses reaching the SC heatwave, however, varied considerably in time.

Figure 3e shows the thermodynamic evolution of these air masses in a potential temperature–temperature diagram. In this diagram, horizontal displacements indicate adiabatic ascent or descent, whereas diabatic heating at constant pressure results in a displacements along the indicated slanted isobars. Figure 3e shows that along all pathways, air masses experienced substantial adiabatic warming of up to 20 K in the median, associated with descent by 150 to 200 hPa. For all air mass sources, diabatic warming remained rather weak, contributing less than 5 K during the final 1–3 days. Similarly, in the CE region, the thermodynamic evolution of the air masses was dominated by adiabatic descent. Nevertheless, air masses from the eastern Atlantic in addition experienced substantial diabatic warming.

At the onset of the CE and concurrent heatwaves, the dominant air mass source for both regions was in the North Atlantic (blue in Figure 3a, c; blue and grey in Figure 3b, d). In both regions, the pathway subsequently changed from west to east (Figure 3). This parallel evolution of the constituent air masses in the concurrent heatwaves suggests that there is a common dynamic driver for both heatwaves.

One obvious candidate for such a common dynamic driver is the Scandinavian block in Figure 2d. However, towards the end of the period of the concurrent

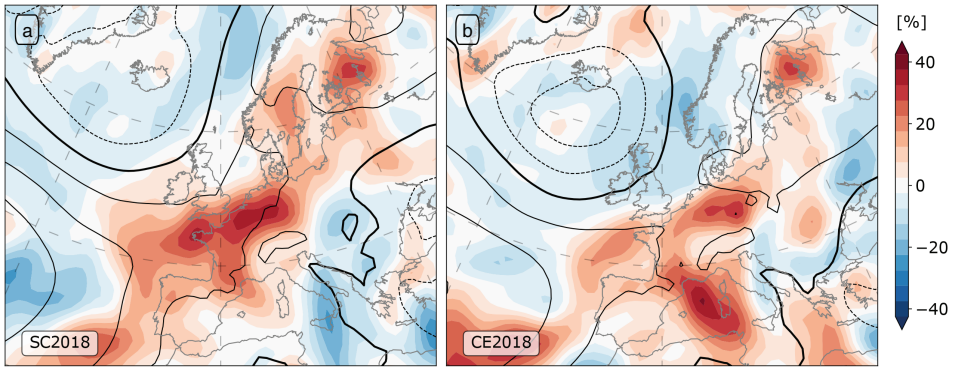

FIGURE 4 Anomalous frequency of occurrence of weak pressure gradients compared to the JJA climatology in Figure 1 (shading, absolute percentages), and average sea level pressure (contour interval 4 hPa with 1,012 hPa bold and dashed below 1,012 hPa) averaged over (a) the 2018 SC heatwave 10 July–4 August and (b) the 2018 CE heatwave 24 July–9 August

heatwaves, this block was displaced northwards and eventually decayed, while the CE heatwave persisted. This decoupling of the heatwave from the block raises the question to what extent the Scandinavian block caused the 2018 CE heatwave. One hint towards an answer lies in the geometrical configuration of the block and the heatwaves. Figure 2 shows that the strongest temperature anomalies and heatwaves tended to occur east of the strongest geopotential gradients in between the trough–ridge couplet, in a region of weak pressure gradients. During both the 2018 SC and CE heatwaves, WPG events were more frequent than in the climatology over Central Europe (Figure 4). The positive frequency anomalies of WPG features over CE were substantial; in some regions they amounted to more than a doubling of the climatological frequency of WPG occurrence (cf. Figures 1 and 4a). Throughout the 2018 heatwaves, these WPG events occurred around the saddle point of a quadrupolar pattern with anticyclones to the northeast and southwest of Central Europe, and cyclonic anomalies to the northwest and, to a lesser extent, the southeast (Figure 4).

4 | THE 2003 SEQUENTIAL HEATWAVE

The record-breaking heatwave in CE in summer 2003 (e.g., Fink *et al.*, 2004; García-Herrera *et al.*, 2010) was preceded by a strong heatwave in Scandinavia (Figure 5). Blocks were present over Scandinavia during both phases of the SC heatwave (Figure 5a–d). In conjunction, they yielded a long-lasting Scandinavian blocking episode from a weather regime perspective (cf. Figure S1a).

The 2003 SC heatwave was abruptly ended by a transition of the large-scale flow in the Euro-Atlantic sector into a new state (Figure 5e,f). During the transition, the block over northern Scandinavia migrated northeastward while at the same time a new block emerged from the North Atlantic (Figure 2d,f). The transition was linked to a deep cyclone, located between Iceland and the British Isles. The cyclone was associated with a strong warm conveyor belt (not shown), whose divergent outflow of low-PV air likely contributed to the build-up of a negative PV anomaly in the upper troposphere and a pronounced ridge over the North Sea (Figure 5g,h) (e.g., Grams *et al.*, 2011; Madonna *et al.*, 2014). This ridge satisfies the criteria for a dynamical block following the Croci-Maspoli *et al.* (2007) definition of a persistent PV anomaly (Figure5h), even though it was not associated with a persistent reversal in the geopotential gradient (not shown).

The evolution of the low-level temperature anomalies clearly shows that no air masses from the SC heatwave were incorporated in the subsequent CE heatwave (Figure 5c,e,g). Instead of being advected towards Central Europe, the air masses were advected northeastward over the Barents Sea, following the flow around the slowly decaying Scandinavian block (Figure 5c,e). This clearly indicates that the CE heatwave formed thermodynamically independent of the preceding SC heatwave.

This interpretation is underlined by the trajectory analysis, in which none of the air stream clusters points to Scandinavia as a source of air masses in CE heatwaves (Figure 6b). Instead, during the onset as well as the second half of the 2003 CE heatwave, most of the trajectories originated from the western Atlantic or the east (blue and grey in Figure 6b,d). In both cases, the air masses descended substantially, but were then also heated diabatically while in the boundary layer (Figure 6e). As the eastern Atlantic contributions became more important throughout the evolution of the CE heatwave, the temperature evolution became again mainly dominated by adiabatic warming (Figure 6d,e).

For the 2003 SC heatwave, the distribution of trajectories amongst the clusters is broadly consistent with the changing synoptic structures during the two phases (Figures 5a–d and 6c). During the onset of both phases, advection from the southwest dominated the air mass composition (Figure 6c). But with the zonal extension of the block (first phase) or gradual movement to the

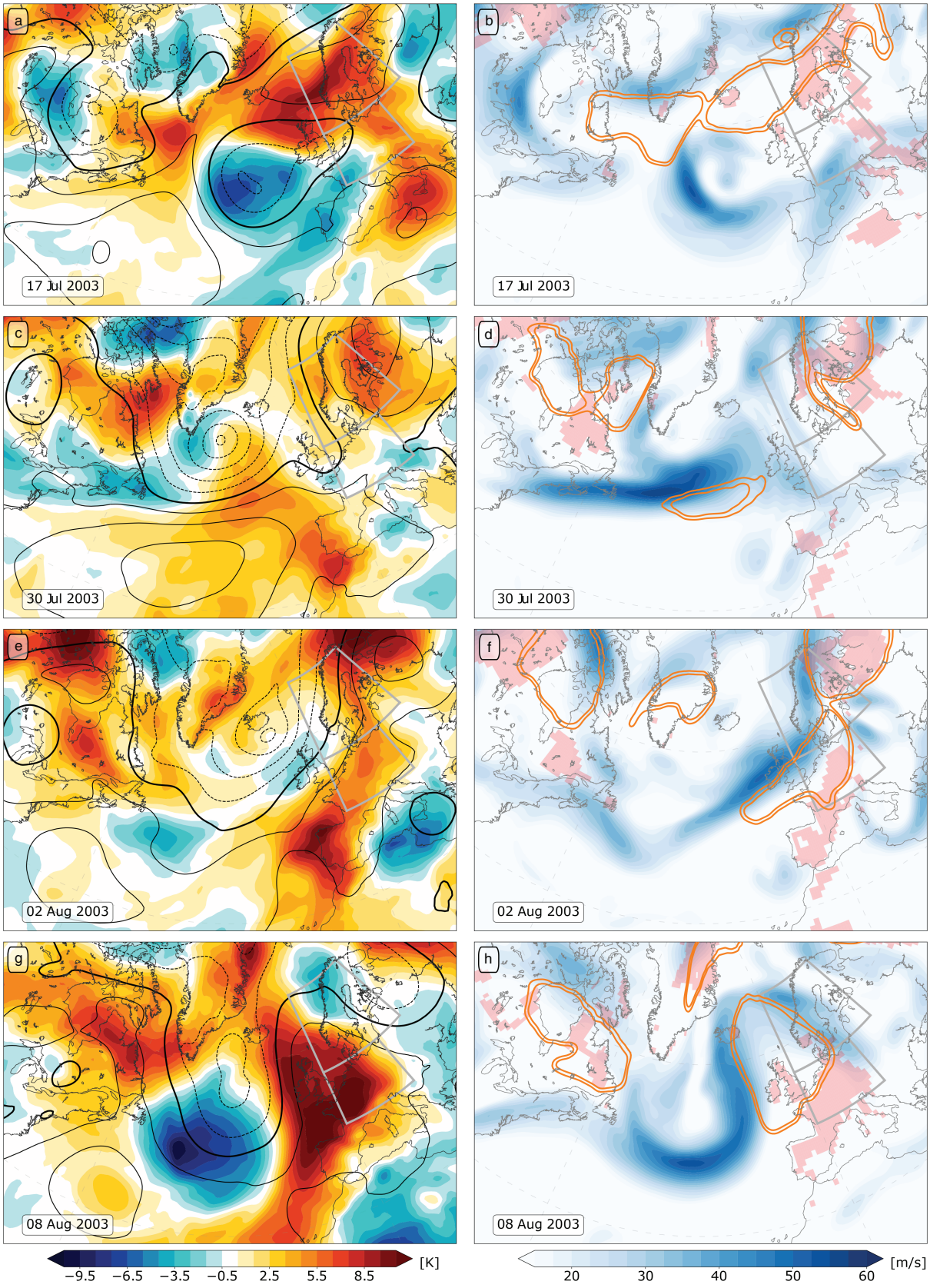

FIGURE 5 As Figure 2, but for the sequential heatwaves of 2003. (a–d) show peaks of the two-part SC heatwave on (a, b) 17 July and (c, d) 30 July. (e, f) show the day of transition (2 August), and (g, h) a peak of the CE heatwave (8 August)

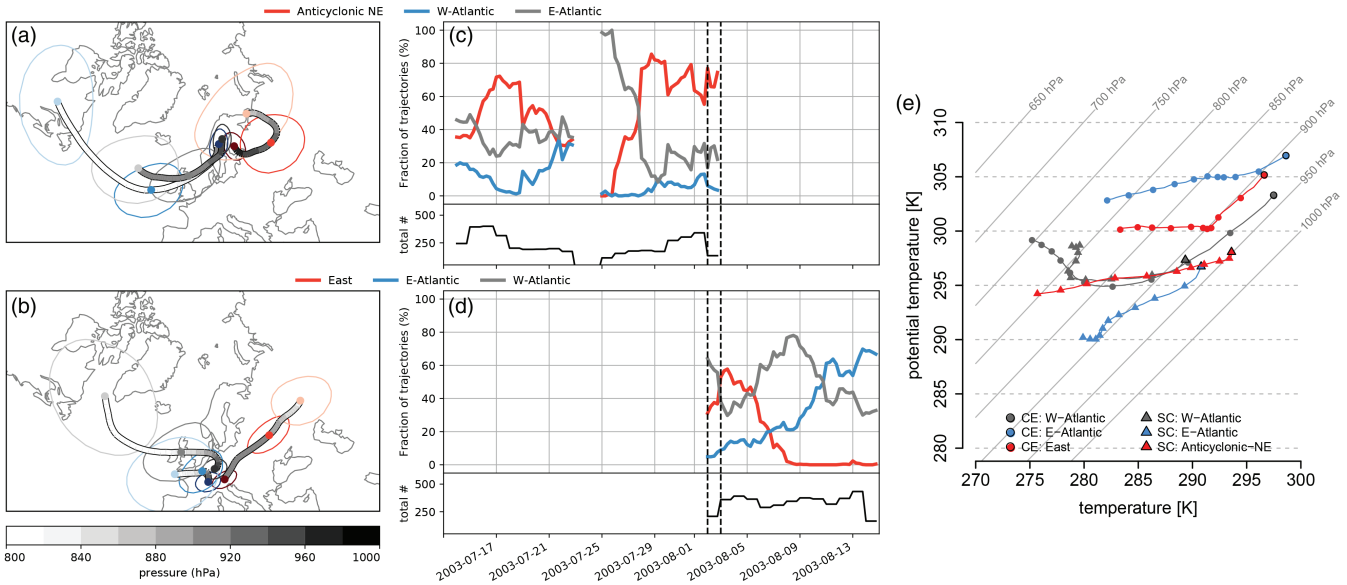

FIGURE 6 As Figure 3 but for the 2003 heatwaves

east (second phase), the air mass composition shifted from predominantly southwesterly to northeasterly flow (Figure 6c).

The changing synoptic structure during the 2003 SC heatwave explains why this heatwave, and the blocks in the Scandinavian region, were hardly associated with WPG events (Figure 7a). During the period of the 2003 SC heatwave, WPG events over Central Europe occurred only marginally more frequently than in the JJA climatology (Figure 7a). However, during the 2003 CE heatwave, WPG events were abundant over Central Europe (Figure 7b). These WPG events are linked to a block over the North Sea and the eastern North Atlantic, but occurred predominantly in a region of reduced synoptic activity outside the perimeter of the block (Figure 5g,h).

5 | SYNTHESIS OF THE CASE-STUDIES AND HEATWAVE CLIMATOLOGY

The discussion of the case-studies indicates some likely answers to the questions we posed initially. (a) The 2018 concurrent heatwaves were related to a Scandinavian blocking episode, (b) the abrupt transition from a SC to CE heatwave in 2003 was associated with an intense cyclone in the central North Atlantic, and (c) we find no indication for recycling of low-level heat in the 2003 case. We now return to these questions in more detail, synthesising our findings for the two case-studies and supplementing them with climatological analyses.

5.1 | WPG events important for CE and concurrent heatwaves

We first consider the dynamics of concurrent heatwaves. In synthesis, the 2003 and 2018 case studies demonstrate that Scandinavian blocks can be associated with a heatwave in Central Europe, but also that this association does not hold for all blocks. For example, the low-level flow pattern during the second phase of the 2003 SC heatwave is similar to the flow during the 2018 SC heatwave (Figures 2a–d and 5c,d). During both events, a prominent trough–ridge couplet leads to low-level southwesterly flow along the Norwegian coast line, and temperature anomalies were most pronounced in central and northern Scandinavia (Figures 2a and 5a). Further, during both events the flow is blocked over Scandinavia (Figures 2b,d and 5d). Nevertheless, only in 2018 did the SC heatwave co-occur with a CE heatwave.

The occurrence of WPG events during these SC heatwaves suggests an explanation for this discrepancy. Whereas WPG events occurred at about the climatological frequency over Central Europe during the 2003 SC heatwave (Figure 7a), they were abundant during the 2018 SC heatwave (Figure 4a). Differences in the location of the Scandinavian block might have caused these differences in WPG event frequency: in 2018 the block was centred over Scandinavia and the Baltic, and in 2003 it was centred over Finland and western Russia. Despite this slight difference in location, the time-average pressure distribution during the two SC heatwaves is remarkably similar (Figures 4a and 7a). The occurrence of WPG events during

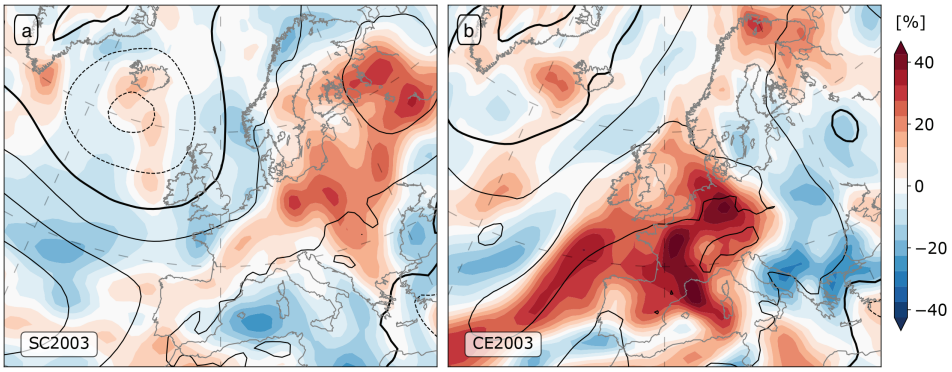

FIGURE 7 As Figure 4, but for (a) the 2003 SC heatwave 14 July–2 August and (b) the 2003 CE heatwave 2–14 August

a given time period thus cannot be deduced from the average sea-level pressure distribution.

The climatological frequencies of WPG events during SC, CE and concurrent heatwaves corroborate our conclusions. While SC heatwaves only exhibit weakly positive anomalies within the centre of a surface anticyclone (Figure 8a), CE and in particular concurrent heatwaves are associated with strongly positive WPG frequency anomalies over Central Europe (Figure 8b,c). Further, the sea-level pressure composite for SC and concurrent heatwaves resemble each other closely, but are associated with very different distributions of WPG events (Figure 8a,c). Here again, the occurrence of WPG events thus provides information not available in the mean sea-level pressure distribution.

Further, the association of CE WPG events and SC blocking provides a plausible dynamical explanation both for the concurrent SC and CE heatwaves in 2018, and for the more general observation that some heatwaves grow beyond the perimeter of the synoptic systems from which they emanate. Following this interpretation, Scandinavian blocks favour both the warm-air advection that we found to be an important contributor to SC heatwaves (trajectory analyses in Figures 3c and 6c), and the occurrence of WPG events with local descent and the gradual build-up of temperature extremes over Central Europe.

The occurrence of heatwaves beyond the perimeter of synoptic systems challenges conventional wisdom about heatwaves, because it questions the one-to-one association of a heatwave to a single synoptic event, be it a block, anticyclone, ridge, Rossby wave breaking event, or Rossby wave packet. For simplicity, we have so far associated the Central European WPG events with the Scandinavian block, but both the 2018 case and the composite show that this block is part of a larger quadrupolar structure with anomalously high pressure to the northeast and southwest, and anomalously low pressure to the northwest and southeast of Central Europe (Figures 4 and 8c). It might thus be misleading to attribute WPG events and CE heatwaves to the Scandinavian block only. Further, as the 2003 case and the CE heatwave composite demonstrate (Figures 7b and 8c), different large-scale flow patterns can have the same effect of suppressing synoptic activity over Central Europe as the mentioned quadrupolar pattern.

5.2 | Dynamics of heatwave transitions

Second, we turn our attention to the synoptic patterns associated with heatwave transitions between Central Europe and Scandinavia. We identified six transitions from CE to SC heatwaves and nine transitions from SC to CE heatwaves in the 40-year climatology. Based on this small database of transitions, we aim to more systematically analyse whether there is a dynamical or thermodynamical link between successions of heatwaves, or whether there is a common dynamical driver upstream in the North Atlantic storm track that triggers the transition.

To this end, we compare composites of heatwave onsets with heatwave transitions, both for Scandinavia (Figure 9) and for Central Europe (Figure 10). Overall, the low-level flow and the pattern of the temperature field look very similar in the onset and transition composites for both regions. For SC heatwaves, the cold anomaly over Greenland is generally much more pronounced during transitions than during onsets (Figure 9a). However the amplitude of the anomaly might only reflect the much smaller sample size of transition cases (6) compared to the overall set of SC onsets (87). The same argument applies to the more pronounced southwesterly advection of warm air over the North Sea towards Scandinavia in the transition cases (Figure 9a). In the upper troposphere, the flow patterns in both composites are quite consistent, albeit again more sharply defined for the transition composite (Figure 9b,d): a rather straight Atlantic jet is directed towards the Iberian peninsula, and a clear signature of blocks is evident over Scandinavia.

The onsets and transitions towards CE heatwaves are associated with a surprisingly similar flow pattern as the

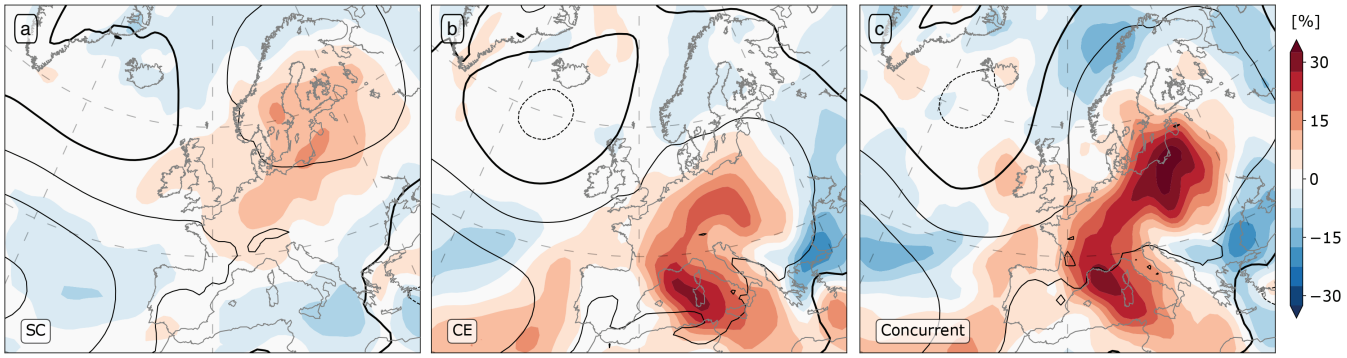

FIGURE 8 Composite anomaly frequency of occurrence of WPG events for all (a) SC heatwave days, (b) CE heatwave days, and (c) concurrent CE and SC heatwave days in the 1979–2018 climatology

onsets and transitions towards SC heatwaves (Figures 9a,c and 10a,c). For onsets in both regions, a trough in the Atlantic steers southwesterly flow over the North Sea, advecting more or less pronounced heat anomalies towards Scandinavia. While the overall geopotential pattern is very similar between SC and CE heatwave onsets, the trough is centred slightly further to the southeast during CE onsets, and the ridge over Scandinavia is considerably more pronounced for SC heatwave onsets. The pronounced trough in the central North Atlantic indicates that cyclonic activity contributes to heatwave onsets in general, but in particular to transition events (Figures 9a,c and 10a,c). This finding is fully in line with our synoptic discussion of the 2003 abrupt transition towards a CE heatwave. There we speculated that cyclonic activity associated with warm conveyor belt activity might have contributed to the formation of the ridge covering Central Europe during the onset of the 2003 CE heatwave.

As expected, the cyclonic activity at low levels is also accompanied at upper levels by a tropopause-level trough (Figures 9b,d and 10b,d). However, with the exception of transitions towards SC heatwaves (Figures 9b), the upper-level flow configuration appears rather diffuse, indicating that different synoptic patterns are entangled in the composite (Figures 9d and 10b,d). Beyond an increased frequency of blocks over Central Europe and Scandinavia and a more-or-less pronounced trough upstream in the North Atlantic, no unique flow structure seems to be associated with either the onset or the transition towards CE and SC heatwaves. Nevertheless, the striking similarity between the transition cases and the onset cases leads us to the conclusion that heatwave transitions should not be regarded as a process distinct from heatwave onsets in general.

5.3 | Concurrent heatwaves more likely than sequential ones

To support the conclusion that heatwave transitions are nothing more than appropriately timed heatwave onsets, we calculate the probability of heatwaves relative to onsets and decays in the neighbouring region (Figure 11). Were there a transition process distinct from a random coincidence of onset and decay, we would expect either a clear increase or decrease in the heatwave probability following a heatwave decay in either region. However, the probability of a heatwave after a decay in the neighbouring region is well within the bounds of statistically independent occurrence (blue line and shading in Figure 11).

In contrast, the probability for an SC heatwave is significantly more likely to occur before the decay (blue line and shading in Figure 11a) and after the onset of a CE heatwave (red line and shading in Figure 11a). Similar tendencies are also evident for the instantaneous likelihood of a CE heatwave relative to SC heatwave onsets and decays (Figure 11b), but the signal is weaker, and the slight increase of CE heatwave probability before a SC heatwave decay is not significant. This asymmetry indicates that weather patterns conducive to heatwaves in Central Europe have a higher influence on Scandinavia than *viceversa*. Nevertheless, the overall conclusion from the analysis in Figure 11 is that concurrent heatwaves are more likely than sequential ones. This conclusion is further supported by the finding that both SC and CE heatwaves are significantly correlated with the occurrence of the Scandinavian blocking weather regime, and, to a lesser extent, the European blocking regime (cf. Figure S2).

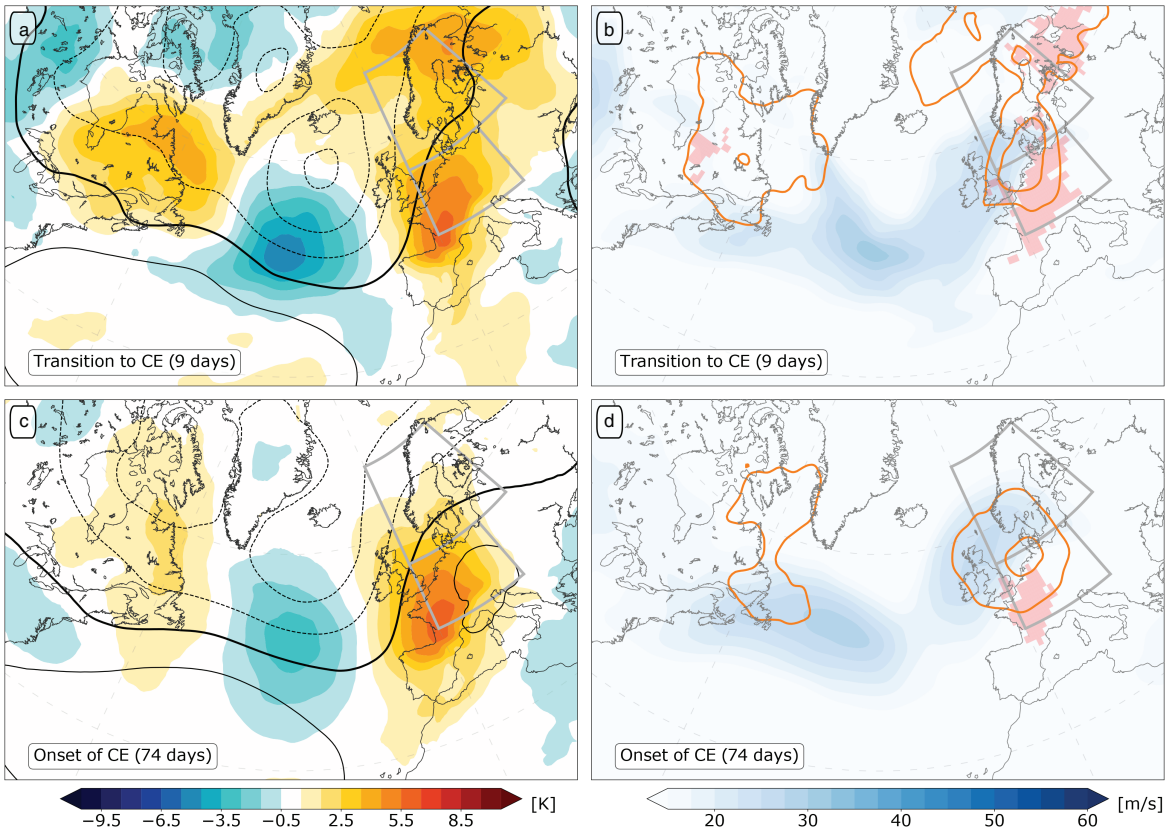

FIGURE 9 As Figure 2, but showing composites for (a, b) transitions from CE to SC heatwaves and (c, d) all onsets of SC heatwaves

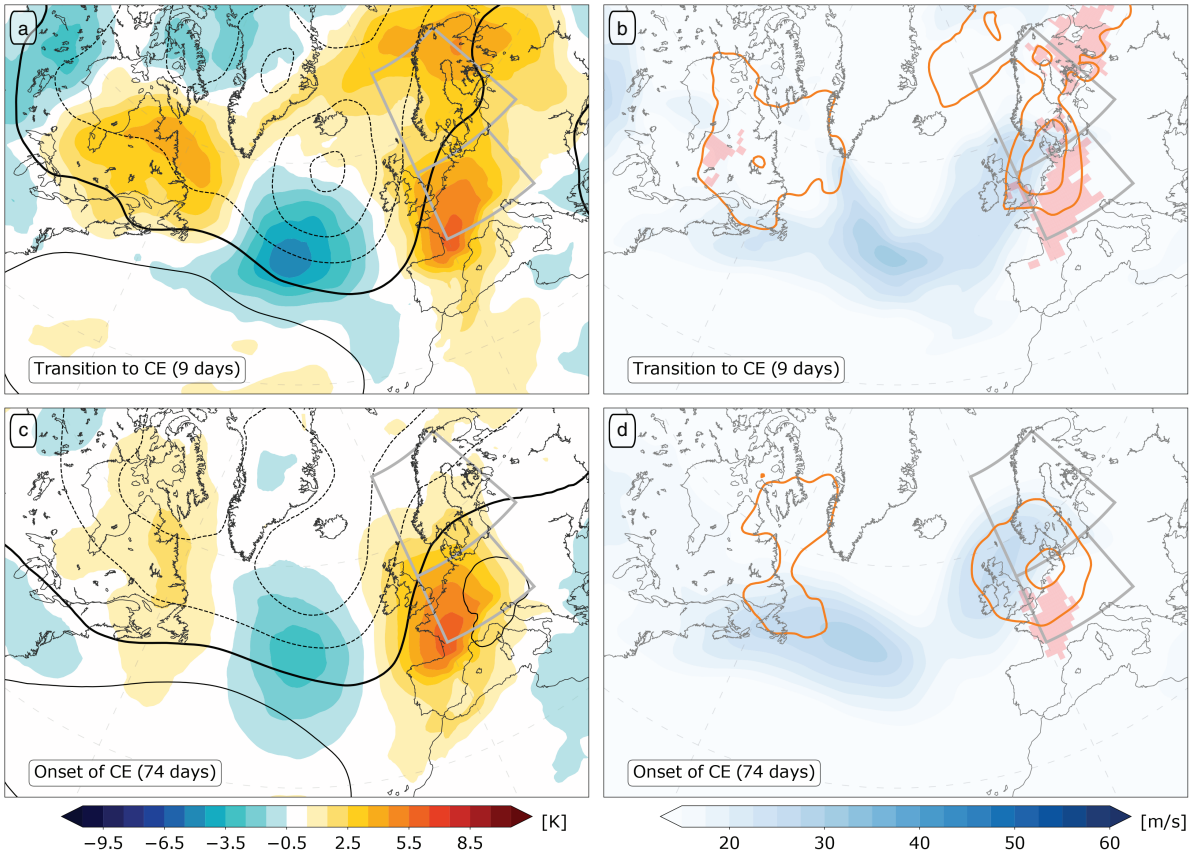

FIGURE 10 As Figure 2, but showing composites for (a, b) transitions from SC to CE heatwaves and (c, d) all onsets of CE heatwaves

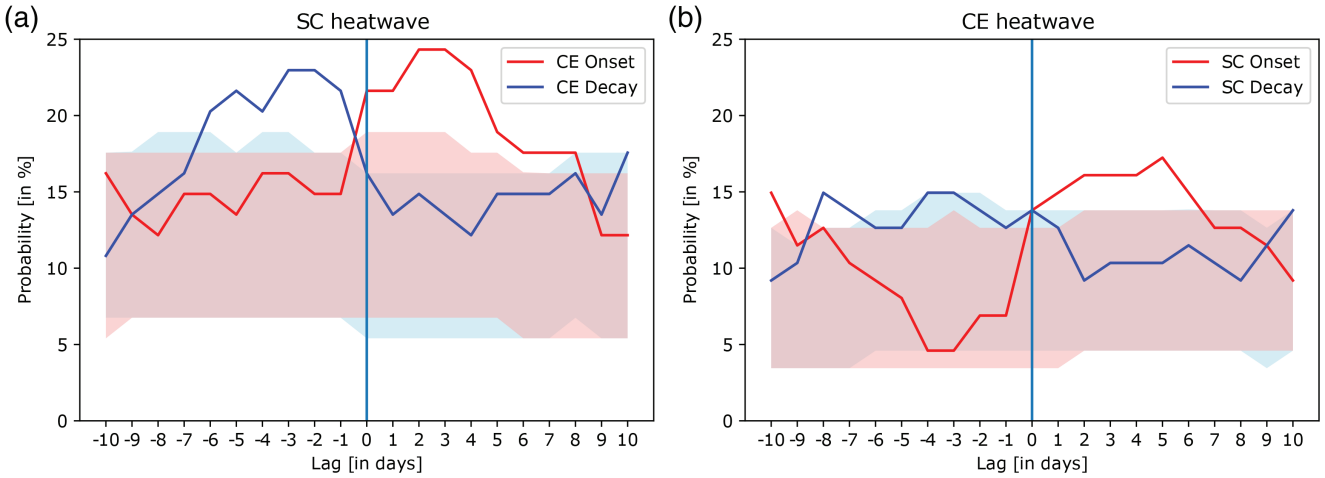

FIGURE 11 Probability of having a heatwave in (a) Scandinavia, and (b) Central Europe before and after the onset and decay of a heatwave in the other region. The shading shows the range of probabilities one would expect of having a heatwave under the the assumption that SC and CE occur independently from each other. Specifically, the shading shows the 5th and 95th percentile of a Monte-Carlo test distribution based on 1,000 resamples of the events in annual chunks. We consider curves outside the respective shading to be a statistically significant deviation from statistically independent occurrence of SC and CE heatwaves

5.4 | Low-level links between heatwaves

Finally, we consider the question of potential low-level links between sequential heatwaves. For sequential heatwaves, the existence of such a link seems unlikely, because we found no indication for a distinct transition process in the climatological composite analysis (Figures 9 and 10), and the occurrence of heatwaves in one region is statistically unrelated to the decay of a heatwave in the other region (Figure 11). The trajectory analysis for the 2003 and 2018 heatwaves underlines this result: none of the typical air mass pathways towards Central Europe leads over Scandinavia, and vice versa (Figures 3a, b and 6a, b). In summary, we find no indication of recycling of low-level heat in sequential heatwaves, neither in the considered case-studies nor in our climatological analyses.

Nevertheless, the trajectory analysis suggests a more indirect connection between Scandinavia and Central Europe. Two of the typical pathways of air masses towards Central Europe as well as one towards Scandinavia lead over the British Isles. And indeed, it is these pathways that dominate the first 4–5 days of the 2018 concurrent heatwaves (Figure 3). Hence, the preferred co-occurrence of SC and CE heatwaves cannot only be related to blocking, or more generally the upper-level flow structure, but also to similar pathways of descending low-level air masses contributing to heatwaves in both regions.

Schumacher *et al.* (2019) provided a second mechanism by which heatwaves in different regions might be connected. They show that in the 2010 Russian heatwave, an upstream soil moisture deficit contributed to the temperature extremes. This mechanism likely did not play an important role for the heatwave cases studied here. In the evolution of potential and actual temperatures along our trajectories shows that adiabatic descent dominates diabatic heating for all source air masses (Figures 3e and 6e). Those trajectories that are affected most by diabatic heating (east Atlantic cluster for the 2018 CE heatwave, west Atlantic cluster for the 2003 CE heatwave) move only slowly in the 5 days preceding the arrival in the heatwave. Slow movement in combination with comparatively large diabatic heating indicates a local build-up of the heat extremes as described by Miralles *et al.* (2014). For the 2018 and 2003 SC heatwaves, diabatic effects account for less than 5 K of heating (Figures 3e and 6e), such that interactions with the land surface can have played only a minor role in these heatwaves.

6 | SUMMARY AND CONCLUSIONS

Based on the analyses presented in this study, we are now in the position to answer the questions raised in the introduction. First, concurrent Central European and Scandinavian heatwaves can to some extent be related to Scandinavian blocking, both in the sense of a synoptic feature and a weather regime. However, neither Central European nor Scandinavian heatwaves are associated one-to-one with Scandinavian blocking. For example, a strong Scandinavian block coincided with the 2018 concurrent heatwaves, and constituted part of a larger-scale flow configuration that suppressed synoptic activity over Central Europe. In contrast, the 2003 Scandinavian heatwave was associated

with several blocks over Scandinavia, none of which led to a heatwave in Central Europe.

Second, the abrupt transition from a Scandinavian to a Central European heatwave in 2003 was associated with a strong summer cyclone in the central North Atlantic. Composite analyses show that the transition from Scandinavian to Central European heatwaves is generally associated with a pronounced trough and cyclone activity in the central North Atlantic. However, this is equally true for onsets of Central European heatwaves in general, and we find no indication of specific dynamical processes that would separate heatwave transitions towards Central Europe from onsets in that region in general. This suggests no particular dynamical link between the heatwaves in the two regions. Further, a co-occurrence of Central European and Scandinavian heatwaves is climatologically more likely than a sequential occurrence.

Third, a trajectory analysis for the 2003 and 2018 cases show hardly any indication of recycling of low-level heat during heatwave transitions. This result is corroborated by our climatological composite analysis and the statistical relation between Scandinavian and Central European heatwaves. In both analyses, "transition events" appear to be merely a random coincidence of a heatwave onset with a heatwave decay in the other region.

In addition, our analyses provide insight into the dynamics of Central European heatwaves. During both 2003 and 2018, the Central European heatwaves occurred without a pronounced anticyclone influencing the region. Rather, the heatwaves were characterised by a synoptic situation associated with nearly vanishing synoptic-scale pressure gradients and winds over Central Europe that allowed the build-up of heat extremes. We refer to these as weak pressure gradient events.

A composite analysis of occurrence of weak pressure gradient events during Central European heatwaves confirms the climatological relation between weak pressure gradient events and Central European heatwaves. Further, the composite analysis shows that weak pressure gradients are particularly prevalent over Central Europe during concurrent heatwaves in Central Europe and Scandinavia. Our definition of WPG events might hence provide a useful diagnostic to further analyse these situations.

Finally, our results provide a basis that might help to bring together the diverging projections for blocking and heatwave frequencies in a warming climate. While blocks themselves may not become more frequent, they can more frequently trigger heatwaves in different regions in their vicinity. To thoroughly establish this link, we require studies examining the influence of global warming on the occurrence of processes relating blocks to heatwaves, such as land-surface and boundary-layer interactions, weak pressure gradient events, and adiabatic descent.

ACKNOWLEDGEMENTS

We thank Heini Wernli for insightful discussions and comments on the manuscript. We thank two anonymous reviewers for their comments, which improved the clarity of the manuscript. We acknowledge MeteoSwiss and the European Centre for Medium Range Weather Forecasting for providing access to the ERA-Interim data. EM was supported by the Bjerknes Centre project EMULATE. MB and MR acknowledge funding of the INTEXseas project from the European Research Council 485 (ERC) under the European Union's Horizon 2020 research and innovation programme (grant agreement No 787652). The contributions of CMG and JFQ are supported by the Helmholtz Association via the Young Investigator Group "SPREADOUT" (grant VH-NG-1243). PZ is funded through the subproject C4 "Coupling of planetray-scale Rossby wave trains to local extremes in heat waves" of the Transregional Collaborative Research Center SFB/TRR 165 "Waves to Weather", funded by the German Research Foundation (DFG).

ORCID

C. Spensberger https://orcid.org/0000-0002-9649-6957
C. M. Grams https://orcid.org/0000-0003-3466-9389
J. F. Quinting https://orcid.org/0000-0002-8409-2541
P. Zschenderlein https://orcid.org/0000-0001-5073-5302

REFERENCES

Barnes, E.A., Dunn-Sigouin, E., Masato, G. and Woollings, T. (2014) Exploring recent trends in Northern Hemisphere blocking. *Geophysical Research Letters*, 41, 638–644.

Barriopedro, D., Fischer, E.M., Luterbacher, J., Trigo, R.M. and García-Herrera, R. (2011) The hot summer of 2010: redrawing the temperature record map of Europe. *Science*, 332, 220–224.

Barriopedro, D., Sousa, P.M., Trigo, R.M., García-Herrera, R. and Ramos, A.M. (2020) The exceptional Iberian heatwave of summer 2018. *Bulletin of the American Meteorological Society*, 101, S29–S34.

Bieli, M., Pfahl, S. and Wernli, H. (2015) A Lagrangian investigation of hot and cold temperature extremes in Europe. *Quarterly Journal of the Royal Meteorological Society*, 141, 98–108.

Black, E., Blackburn, M., Harrison, G., Hoskins, B.J. and Methven, J. (2004) Factors contributing to the summer 2003 European heatwave. *Weather*, 59, 217–223.

Cassou, C., Terray, L. and Phillips, A.S. (2005) Tropical atlantic influence on European heat waves. *Journal of Climate*, 18, 2805–2811.

Cattiaux, J., Quesada, B., Arakélian, A., Codron, F., Vautard, R. and Yiou, P. (2013) North Atlantic dynamics and European

temperature extremes in the IPSL model: sensitivity to atmospheric resolution. *Climate Dynamics*, 40, 2293–2310.

Cattiaux, J. and Ribes, A. (2018) Defining single extreme weather events in a climate perspective. *Bulletin of the American Meteorological Society*, 99, 1557–1568.

Christidis, N., Jones, G.S. and Stott, P.A. (2015) Dramatically increasing chance of extremely hot summers since the 2003 European heatwave. *Nature Climate Change*, 5, 46

Coumou, D. and Robinson, A. (2013) Historic and future increase in the global land area affected by monthly heat extremes. *Environmental Research Letters*, 8, 034018

Croci-Maspoli, M., Schwierz, C. and Davies, H.C. (2007) A multifaceted climatology of atmospheric blocking and its recent linear trend. *Journal of Climate*, 20, 633–649.

De Bono, A., Giuliani, G., Kluser, S. and Peduzzi, P. (2004). Impacts of summer 2003 heat wave in Europe. Environment Alert Bulletin, UNEP, Nairobi, https://www.unisdr.org/files/1145_ewheatwave.en.pdf; accessed 19 May 2020.

Dee, D.P., Uppala, S.M., Simmons, A.J., Berrisford, P., Poli, P., Kobayashi, S., Andrae, U., Balmaseda, M.A., Balsamo, G., Bauer, P., Bechtold, P., Beljaars, A.C.M., van de Berg, L., Bidlot, J., Bormann, N., Delsol, C., Dragani, R., Fuentes, M., Geer, A.J., Haimberger, L., Healy, S.B., Hersbach, H., Hólm, E.V., Isaksen, L., Kållberg, P., Köhler, M., Matricardi, M., McNally, A.P., Monge-Sanz, B.M., Morcrette, J.-J., Park, B.-K., Peubey, C., de Rosnay, P., Tavolato, C., Thépaut, J.-N. and Vitart, F. (2011) The ERA-Interim reanalysis: configuration and performance of the data assimilation system. *Quarterly Journal of the Royal Meteorological Society*, 137, 553–597.

Della-Marta, P.M., Luterbacher, J., von Weissenfluh, H., Xoplaki, E., Brunet, M. and Wanner, H. (2007) Summer heat waves over western Europe 1880–2003, their relationship to large-scale forcings and predictability. *Climate Dynamics*, 29, 251–275.

Dole, R., Hoerling, M., Perlwitz, J., Eischeid, J., Pegion, P., Zhang, T., Quan, X.-W., Xu, T. and Murray, D. (2011) Was there a basis for anticipating the 2010 Russian heat wave?. *Geophysical Research Letters*, 38(6). https://doi.org/10.1029/2010GL046582

Drouard, M., Kornhuber, K. and Woollings, T. (2019) Disentangling dynamic contributions to summer 2018 anomalous weather over Europe. *Geophysical Research Letters*, 46(21), 12537–12546. https://doi.org/10.1029/2019GL084601

Drouard, M. and Woollings, T. (2018) Contrasting mechanisms of summer blocking over western Eurasia. *Geophysical Research Letters*, 45(21), 12040–12048. https://doi.org/10.1029/2018GL079894

Fink, A.H., Brücher, T., Krüger, A., Leckebusch, G.C., Pinto, J.G. and Ulbrich, U. (2004) The 2003 European summer heatwaves and drought – synoptic diagnosis and impacts. *Weather*, 59, 209–216.

Fischer, E.M. (2014) Climate science: autopsy of two mega-heatwaves. *Nature Geoscience*, 7, 332–333. https://doi.org/10.1038/ngeo2148

Fischer, E.M. and Schär, C. (2010) Consistent geographical patterns of changes in high-impact European heatwaves. *Nature Geoscience*, 3, 398–403. https://doi.org/10.1038/ngeo866

Fischer, E.M., Seneviratne, S.I., Lüthi, D. and Schär, C. (2007) Contribution of land–atmosphere coupling to recent European summer heat waves. *Geophysical Research Letters*, 34(6). https://doi.org/10.1029/2006GL029068

Fragkoulidis, G., Wirth, V., Bossmann, P. and Fink, A.H. (2018) Linking Northern Hemisphere temperature extremes to Rossby wave packets. *Quarterly Journal of the Royal Meteorological Society*, 144, 553–566.

García-Herrera, R., Díaz, J., Trigo, R.M., Luterbacher, J. and Fischer, E.M. (2010) A review of the European summer heat wave of 2003. *Critical Reviews in Environmental Science and Technology*, 40, 267–306. https://doi.org/10.1080/10643380802238137

Grams, C.M., Beerli, R., Pfenninger, S., Staffell, I. and Wernli, H. (2017) Balancing Europe's wind-power output through spatial deployment informed by weather regimes. *Nature Climate Change*, 7, 557–562. https://doi.org/10.1038/nclimate3338

Grams, C.M., Wernli, H., Boettcher, M., Čampa, J., Corsmeier, U., Jones, S.C., Keller, J.H., Lenz, C.-J. and Wiegand, L. (2011) The key role of diabatic processes in modifying the upper-tropospheric wave guide: a North Atlantic case-study. *Quarterly Journal of the Royal Meteorological Society*, 137, 2174–2193.

Hart, N.C.G., Gray, S.L. and Clark, P.A. (2015) Detection of coherent airstreams using cluster analysis: Application to an extratropical cyclone. *Monthly Weather Review*, 143, 3518–3531.

Horton, R.M., Mankin, J.S., Lesk, C., Coffel, E. and Raymond, C. (2016) A review of recent advances in research on extreme heat events. *Current Climate Change Reports*, 2, 242–259.

Hoskins, B.J. (1975) The geostrophic momentum approximation and the semi-geostrophic equations. *Journal of the Atmospheric Sciences*, 32, 233–242.

Jézéquel, A., Cattiaux, J., Naveau, P., Radanovics, S., Ribes, A., Vautard, R., Vrac, M. and Yiou, P. (2018a) Trends of atmospheric circulation during singular hot days in Europe. *Environmental Research Letters*, 13. https://doi.org/10.1088/1748-9326/aab5da

Jézéquel, A., Yiou, P. and Radanovics, S. (2018b) Role of circulation in European heatwaves using flow analogues. *Climate Dynamics*, 50, 1145–1159.

Kennedy, J.J., Killick, R.E., Dunn, R.J., McCarthy, M.P., Morice, C.P., Rayner, N.A. and Titchner, H.A. (2019) Global and regional climate in 2018. *Weather*, 74, 332–340.

Kornhuber, K., Osprey, S., Coumou, D., Petri, S., Petoukhov, V., Rahmstorf, S. and Gray, L.J. (2019) Extreme weather events in early summer 2018 connected by a recurrent hemispheric wave-7 pattern. *Environmental Research Letters*, 14(5). https://doi.org/10.1088/1748-9326/ab13bf

Lesk, C., Rowhani, P. and Ramankutty, N. (2016) Influence of extreme weather disasters on global crop production. *Nature*, 529, 84–87. https://doi.org/10.1038/nature16467

Luterbacher, J., Dietrich, D., Xoplaki, E., Grosjean, M. and Wanner, H. (2004) European seasonal and annual temperature variability, trends, and extremes since 1500. *Science*, 303, 1499–1503.

Madonna, E., Wernli, H., Joos, H. and Martius, O. (2014) Warm conveyor belts in the ERA-Interim dataset (1979–2010). Part I: climatology and potential vorticity evolution. *Journal of Climate*, 27, 3–26.

Magnusson, L., Ferranti, L. and Vamborg, F. (2018) Forecasting the 2018 European heatwave. *ECMWF Newsletter*, 157, 2–3.

Meehl, G.A. and Tebaldi, C. (2004) More intense, more frequent, and longer lasting heat waves in the 21st century. *Science*, 305, 994–997.

Michel, C. and Rivière, G. (2011) The link between Rossby wave breakings and weather regime transitions. *Journal of the Atmospheric Sciences*, 68, 1730–1748.

Miralles, D.G., Teuling, A.J., Van Heerwaarden, C.C. and de Arellano, J.V.-G. (2014) Mega-heatwave temperatures due to combined soil

desiccation and atmospheric heat accumulation. *Nature Geoscience*, 7, 345–349. https://doi.org/10.1038/ngeo2141

Nabizadeh, E., Hassanzadeh, P., Yang, D. and Barnes, E.A. (2019) Size of the atmospheric blocking events: Scaling law and response to climate change. *Geophysical Research Letters*, 46, 13488–13499. https://doi.org/10.1029/2019GL084863

Perkins, S.E. (2015) A review on the scientific understanding of heatwaves – their measurement, driving mechanisms, and changes at the global scale. *Atmospheric Research*, 164, 242–267.

Pfahl, S. and Wernli, H. (2012) Quantifying the relevance of atmospheric blocking for co-located temperature extremes in the Northern Hemisphere on (sub-) daily time scales. *Geophysical Research Letters*, 39(12). https://doi.org/10.1029/2012GL052261

Quinting, J.F., Parker, T. and Reeder, M. (2018) Two synoptic routes to subtropical heat waves as illustrated in the Brisbane region of Australia. *Geophysical Research Letters*, 45, 10700–10708.

Quinting, J.F. and Reeder, M.J. (2017) Southeastern Australian heat waves from a trajectory viewpoint. *Monthly Weather Review*, 145, 4109–4125.

Robine, J.-M., Cheung, S.L.K., Le Roy, S., Van Oyen, H., Griffiths, C., Michel, J.-P. and Herrmann, F.R. (2008) Death toll exceeded 70,000 in Europe during the summer of 2003. *Comptes Rendus Biologies*, 331, 171–178.

Röthlisberger, M., Frossard, L., Bosart, L.F., Keyser, D. and Martius, O. (2019) Recurrent synoptic-scale Rossby wave patterns and their effect on the persistence of cold and hot spells. *Journal of Climate*, 32, 3207–3226.

Russo, S., Dosio, A., Graversen, R.G., Sillmann, J., Carrao, H., Dunbar, M.B., Singleton, A., Montagna, P., Barbola, P. and Vogt, J.V. (2014) Magnitude of extreme heat waves in present climate and their projection in a warming world. *Journal of Geophysical Research: Atmospheres*, 119, 12500–12512.

Russo, S., Sillmann, J. and Fischer, E.M. (2015) Top ten European heatwaves since 1950 and their occurrence in the coming decades. *Environmental Research Letters*, 10(12). https://doi.org/10.1088/1748-9326/10/12/124003

Sánchez-Benítez, A., García-Herrera, R., Barriopedro, D., Sousa, P.M. and Trigo, R.M. (2018) June 2017: the earliest European summer mega-heatwave of reanalysis period. *Geophysical Research Letters*, 45, 1955–1962.

Schaller, N., Sillmann, J., Anstey, J.A., Fischer, E.M., Grams, C.M. and Russo, S. (2018) Influence of blocking on Northern European and Western Russian heatwaves in large climate model ensembles. *Environmental Research Letters*, 13(5). https://doi.org/10.1088/1748-9326/aaba55

Schär, C. and Jendritzky, J. (2004) Hot news from summer 2003. *Nature*, 432, 559–560.

Schumacher, D.L., Keune, J., Van Heerwaarden, C.C., Vilà-guerau De Arellano, J., Teuling, A.J. and Miralles, D.G. (2019) Amplification of mega-heatwaves through heat torrents fuelled by upwind drought. *Nature Geoscience*, 12, 712–717. https://doi.org/10.1038/s41561-019-0431-6

Sinclair, V.A., Mikkola, J., Rantanen, M. and Räisänen, J. (2019) The summer 2018 heatwave in Finland. *Weather*, 74, 403–409.

Sousa, P.M., Trigo, R.M., Barriopedro, D., Soares, P.M.M. and Santos, J.A. (2018) European temperature responses to blocking and ridge regional patterns. *Climate Dynamics*, 50, 457–477.

Sprenger, M., Fragkoulidis, G., Binder, H., Croci-Maspoli, M., Graf, P., Grams, C.M., Knippertz, P., Madonna, E., Schemm, S., Škerlak, B. and Wernli, H. (2017) Global climatologies of Eulerian and Lagrangian flow features based on ERA-Interim. *Bulletin of the American Meteorological Society*, 98, 1739–1748.

Sprenger, M. and Wernli, H. (2015) The LAGRANTO Lagrangian analysis tool – version 2.0. *Geoscientific Model Development*, 8, 2569–2586.

Stefanon, M., D'Andrea, F. and Drobinski, P. (2012) Heatwave classification over Europe and the Mediterranean region. *Environmental Research Letters*, 7. https://doi.org/10.1088/1748-9326/7/1/014023

The Local (2018) What you need to know about Sweden's historic wildfire outbreak. *The Local; Sweden's news in English*. https://www.thelocal.se/20180717/; accessed 17 September 2019

Trigo, R., Trigo, I., DaCamara, C. and Osborn, T. (2004) Climate impact of the European winter blocking episodes from the NCEP/NCAR reanalyses. *Climate Dynamics*, 23, 17–28.

Trigo, R.M., García-Herrera, R., Díaz, J., Trigo, I.F. and Valente, M.A. (2005) How exceptional was the early August 2003 heatwave in France?. *Geophysical Research Letters*, 32(10). https://doi.org/10.1029/2005GL022410

Vautard, R., Yiou, P., D'andrea, F., De Noblet, N., Viovy, N., Cassou, C., Polcher, J., Ciais, P., Kageyama, M. and Fan, Y. (2007) Summertime European heat and drought waves induced by wintertime Mediterranean rainfall deficit. *Geophysical Research Letters*, 34(7). https://doi.org/10.1029/2006GL028001

Vogel, M.M., Zscheischler, J., Wartenburger, R., Dee, D. and Seneviratne, S.I. (2019) Concurrent 2018 hot extremes across Northern Hemisphere due to human-induced climate change. *Earth's Future*, 7, 692–703.

Wernli, H. and Davies, H.C. (1997) A Lagrangian-based analysis of extratropical cyclones. I: the method and some applications. *Quarterly Journal of the Royal Meteorological Society*, 123, 467–489.

Wolf, G. and Wirth, V. (2015) Implications of the semi-geostrophic nature of Rossby waves for Rossby wave packet detection. *Monthly Weather Review*, 143, 26–38.

Woollings, T., Barriopedro, D., Methven, J., Son, S.-W., Martius, O., Harvey, B., Sillmann, J., Lupo, A.R. and Seneviratne, S. (2018) Blocking and its response to climate change. *Current Climate Change Reports*, 4, 287–300.

Zschenderlein, P., Fink, A.H., Pfahl, S. and Wernli, H. (2019) Processes determining heat waves across different European climates. *Quarterly Journal of the Royal Meteorological Society*, 145, 2973–2989.

SUPPORTING INFORMATION

Additional supporting information may be found online in the Supporting Information section at the end of this article.

How to cite this article: Spensberger C, Madonna E, Boettcher M, *et al*. Dynamics of concurrent and sequential Central European and Scandinavian heatwaves. *Q.J.R. Meteorol. Soc*. 2020;146:2998–3013. https://doi.org/10.1002/qj.3822